DOI：10. 13471/j. cnki. acta. snus. ZR20240347

# A dual-emission carbon dots-based ratiometric sensor for detection and cellular imaging of $Mn^{2+}$ ions*

*ZHANG Yuecheng*[1], *MA Jing*[1], *SUN Lingbo*[2]✉, *CHEN Fei*[3], *ZHANG Shiyu*[1], *ZHANG Yuhan*[2], *LI Miao*[1], *ZHANG Yarong*[1], *MA Hongyan*[1]

*1. College of Chemistry and Chemical Engineering, Yan'an University, Yan'an 716000, China*
*2. Medical College of Yan'an University, Yan'an University, Yan'an 716000, China*
*3. Xinzheng Inspection and Testing Co., Ltd, Urumqi 830000, China*

**Abstract:** Manganese (Mn), an essential trace element in the human body, plays critical roles in many biological processes. Recent studies have discovered that $Mn^{2+}$ may promote or directly activate the cGAS-STING pathway, thereby subsequently initiating the natural immune response and augmenting antitumor therapy. However, the current lack of accurate methods for $Mn^{2+}$ determination in cells significantly limits their mechanism investigation; hence, it is urgent to establish novel tools to detect $Mn^{2+}$ in cells. In this study, the dual-emission carbon dots were initially synthesized via the one-pot hydrothermal method employing *L*-aspartic acid and *p*-phenylenediamine as raw materials. In the presence of $Mn^{2+}$, the emission peak centered at 350 nm exhibited significant enhancement, whereas another peak at 610 nm remained stable. Consequently, a ratiometric sensor for $Mn^{2+}$ determination was established using the signal at 350 nm as the responsive signal and the signal at 610 nm as an internal reference. Under the optimal condition, a good linear relationship was achieved between the $F_{350}/F_{610}$ value and $Mn^{2+}$ concentration ranging from 0.9 to 15 μmol/L, with a calculated LOD of 61 nmol/L. Benefiting from the special $Mn^{2+}$-induced ratiometric approach, this method demonstrates outstanding sensitivity, selectivity, and stability, rendering it applicable for $Mn^{2+}$ determination in complex biological samples, as well as $Mn^{2+}$ imaging in MKN-45 and LO2 cells.

**Key words:** $Mn^{2+}$; carbon dots; ratiometric; cell imaging; fluorescence
**CLC number:** O65 **Document code:** A **Article ID:** 2097 − 0137(2025)03 − 0060 − 14

Manganese (Mn) is an essential trace element in the human body, and more than 95% of Mn in cells is stored in the mitochondria and Golgi apparatus with +2 form (Horning et al. , 2015). $Mn^{2+}$ plays a critical role in many biological processes. For instance, $Mn^{2+}$ can act as a cofactor for many enzymes, including

* **Received**: 2024 − 12 − 08 **Accepted**: 2024 − 12 − 23 **Published online**: 2025 − 01 − 21
**Supported by** National Natural Science Foundation of China (22264023); Natural Science Foundation of Shaanxi Province (2024JC-YBQN-0150); Yan'an Science and Technology Bureau Project (2023-SFGG-057); Scientific Research Projects of Education Department of Shaanxi Province (22JK0614); PhD Start Fund of Yan'an University (YDBK2022-15)

✉ **Corresponding author**: SUN Lingbo(*lingbosun@yau.edu.cn*)
ZHANG Yuecheng(*yuechengzhang@yau.edu.cn*); MA Jing(*majing@yau.edu.cn*);
CHEN Fei(*ilucy123@126.com*); ZHANG Shiyu(*zsywhz0223@yau.edu.cn*);
ZHANG Yuhan(*z13201471702@outlook.com*); LI Miao(*18932826802@yau.edu.cn*);
ZHANG Yarong(*zhangyarong@yau.edu.cn*); MA Hongyan(*mahy6614@yau.edu.cn*)

manganese superoxide dismutase, manganese catalase and peroxidase (Fan et al. , 2023). $Mn^{2+}$ also shows high importance for the nervous system and an excess of $Mn^{2+}$ can cause irreversible damage, leading to various neurological diseases such as manganese poisoning, Parkinson's syndrome, and cognitive dysfunction (Kwakye et al. , 2015; Li et al. , 2018). Besides, as a natural agonist, $Mn^{2+}$ could promote or directly activate the cGAS-STING pathway (Lv et al. , 2020), subsequently activating the natural immune response and enhancing the antitumor therapy. Based on its great potential for application in immunotherapy, an increasing number of Mn-based nanomaterials have been synthesized and applied for antitumor therapy (Cai et al. , 2023; Shi et al. , 2023). However, due to the lack of specific probes for $Mn^{2+}$ analysis, its detailed mechanism in immunotherapy is still unclear. Therefore, it is urgent to establish sensitive and selective methods for $Mn^{2+}$ analysis, which can be further applied to investigate the mechanism of $Mn^{2+}$-mediated immune regulation.

Currently, many methods have been established for $Mn^{2+}$ determination, including atomic absorption spectrometry, colorimetric, and chemiluminescence method (Pourjavid et al. , 2016; Zhang et al. , 2022). Although these methods achieve accurate $Mn^{2+}$ analysis in solution, they fail to probe the spatial location and distribution of $Mn^{2+}$ in cells and biological systems, thereby significantly limits their application in the mechanism investigation. As a powerful tool for target analysis and cell imaging, fluorescence has received widespread attention due to its high sensitivity and selectivity (Wang et al. , 2024). However, for the fluorescence probe of $Mn^{2+}$, a major challenge was that paramagnetic $Mn^{2+}$ ions could efficiently quench fluorophores (Mizunuma et al. , 2023), which were not suitable for $Mn^{2+}$ analysis in biological systems and cell imaging. Besides, $Mn^{2+}$ lies at the bottom of the Irving-Williams series ($Mn^{2+}<Fe^{2+}<Co^{2+}<Ni^{2+}<Cu^{2+}>Zn^{2+}$), which means that the stability of forming $Mn^{2+}$ complexes with common ligands is weaker than other divalent metal ions (Das et al. , 2019). Therefore, it is still a great challenge to construct a specific fluorescence sensor to probe and analyze $Mn^{2+}$ distribution in cells and biological systems.

Carbon dots (CDs) is a new member of carbon-based photoluminescence materials which were first discovered in 2004. Compared with traditional semiconductor quantum dots and organic dyes, CDs have received considerable attention due to their numerous merits, such as excellent biological compatibility, fascinating optical properties and low toxicity (Tuerhong et al. , 2017). The surface of CDs contains a rich number of functional groups which can provide abundant binding sites for specific analytes (Chaudhari et al. , 2024; Zhang et al. , 2024). This property makes CDs one of the ideal materials for the sensing process. Besides, the fluorescence properties of CDs are closely related to their surface structure, and the binding of analyte on the surface would directly change the surface structure, thus affecting the CDs emission spectrum, which could be further applied for analyte determination (Zhang et al. , 2021). Based on this, Mohagheghpour et al. (2022) synthesized the histidine-functionalized carbon quantum dots by using histidine and sodium citrate as raw materials. In the presence of $Mn^{2+}$, the signal at 534 nm was significantly increased, thus the fluorescence "turn-on" responsive sensor was established. By using a similar approach, Ngeontae et al. (2022) synthesized the N,S-doped carbon dots and established a highly selective fluorescence sensor for $Mn^{2+}$ analysis. However, the sensing process of these methods only relies on the signal change from a single wavelength, which may be affected by different factors, including the local probe concentration, unstable light source and microenvironment (Wang et al. , 2016). These factors may cause the inability of the quantitative determinations. The ratiometric approach is one of the best ways to overcome these problems by using the ratio of fluorescence intensity from at least two well-resolved wavelengths. Through involving an internal reference, the ratiometric approach can effectively eliminate background signals and environmental interference, thus providing an accurate quantitative and qualitative analysis (Goshisht et al. , 2023; Chen et al. , 2024).

To construct the CDs-based ratiometric assay, one of the most effective approaches is to directly synthesize CDs with dual-emission properties. Therefore, the dual-emissive CDs (DE-CDs) with unique dual-emission properties were first synthesized in this work by using *L*-aspartic acid and *p*-phenylenediamine (*p*-PD) as raw materials. As shown in Fig. 1, under the excitation of 290 nm, as-synthesized DE-CDs exhibit two well-resolved peaks centered at 350 and 610 nm, respectively. In the presence of $Mn^{2+}$, $Mn^{2+}$ specifically conjugated on the surface of DE-CDs, consequently enhanced the fluorescence signal at 350 nm, while the intensity at 610 nm kept stable. Thus, a simple ratiometric approach for $Mn^{2+}$ determination was established by using the fluorescence signal at 350 nm as the responsive signal and the signal at 610 nm as the internal reference. Interestingly, the paramagnetic $Mn^{2+}$ ions did not quench the signal; on the contrary, enhanced the signal at 350 nm. To the best of our knowledge, this is the first time to establish a CDs-based ratiometric $Mn^{2+}$ sensor with an enhanced signal. Benefiting from this special $Mn^{2+}$-induced ratiometric approach, this method exhibits excellent sensitivity, selectivity, and stability, which could be further applied for $Mn^{2+}$ determination in complex biological samples and cellular imaging.

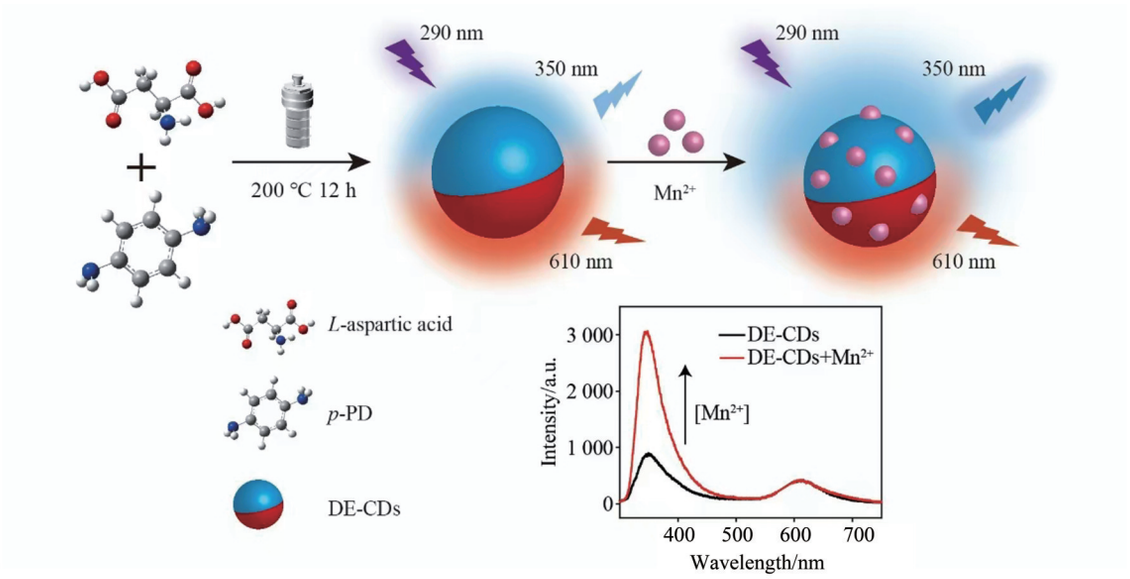


Fig. 1 The scheme for synthesis of DE-CDs and their application in the determination of $Mn^{2+}$

## 1 Materials and methods

### 1. 1 Chemical Reagents and Cells Culture

The *p*-PD, *o*-PD and *m*-PD were purchased from Aladdin Biochemical Technology Co. , Ltd (Shanghai, China). *L*-aspartic acid was brought from Sangon Biotech Co. , Ltd. (Shanghai, China). $MnSO_4$ was obtained from the Jiaozuo Chemical Factory (Jiaozuo, China). Cell Counting Kit-8 (CCK-8) was purchased from Shandong Topscience Biotech Co. , Ltd. (Rizhao, China). The fetal bovine serum (FBS) and cell culture medium were obtained from Biological Industries Ltd. (Beit Haemek, Israel). All other reagents used in this experiment were analytical grade and used as received, and the water was purified by a Milli-Q filtration system. Human cell lines MKN-45 and LO2 were obtained from Procell Life Science & Technology Co. , Ltd. (Wuhan, China). MKN-45 is a human gastric cancer cell line cultured in Dulbecco's Modified Eagle Medium (DMEM) supplemented with 10% FBS. LO2 is a human hepatic cell line cultured in Roswell Park Memorial Institute (RPMI) 1640 medium supplemented with 10% FBS. Both cell lines were cultured at 37 ℃ with 5% $CO_2$ in 100% humidity.

### 1. 2 Synthesis of DE-CDs and control CDs

The CDs were synthesized through the one-pot hydrothermal method. Briefly, a mixture comprising *L*-aspartic acid (0. 005 3 g) and *p*-PD (0. 030 0 g) was

homogenized and solubilized in 20 mL of aqueous solution. Subsequently, the resulting mixture was transferred into a Teflon autoclave and subjected to heating at 200 ℃ for 12 h. Upon reaching ambient temperature, the resultant dark-brown amalgamation underwent purification utilizing filter paper in conjunction with a 0.22 μm filter to eliminate oversized particulates. After that, this mixture was further diluted to 100 mL with ultrapure water and stored at 4 ℃ for further use. For control CDs synthesis, commonly employed raw materials such as *o*-PD, *m*-PD, ethylenediamine, glutathione, and formamide were employed as precursors to substitute *p*-PD. Apart from the altered precursors, all other synthesis conditions remained consistent with those of DE-CDs.

### 1.3 Standard analysis procedure for $Mn^{2+}$

Within the standardized $Mn^{2+}$ analysis protocol, a 1 mL amalgam comprising 200 μL of freshly synthesized DE-CDs, 30 μL of Tris-HCl buffer (pH=7.00), and variable concentration of $Mn^{2+}$ was incubated at room temperature for 10 mins. Subsequently, the fluorescence emission spectrum was interrogated following excitation at 290 nm, with the fluorescence intensities at 350 and 610 nm being meticulously documented.

### 1.4 Specificity test of the constructed ratiometric assay

The specificity of the constructed assay was tested with several different cations and anions, including $Ca^{2+}$, $Mg^{2+}$, $Na^{+}$, $K^{+}$, $Zn^{2+}$, $Ba^{2+}$, $Pb^{2+}$, $Co^{2+}$, $Cd^{2+}$, $F^{-}$, $Br^{-}$, $I^{-}$ and $ClO^{-}$. These studies were carried out using similar procedures to the standard procedure for $Mn^{2+}$ analysis stated above, except that 20 μmol/L interferent was added to the system instead of $Mn^{2+}$. Furthermore, to estimate the interference of cations and biomolecules commonly involved in cell medium and biological systems, $Mn^{2+}$ coexisted with different interferents (fixed at 700 μmol/L) which is 100 times higher than that of $Mn^{2+}$.

### 1.5 *In vitro* cell viability by CCK-8 Assay

The human gastric cancer cell line MKN-45 was employed for the assessment of cellular viability. MKN-45 cells in logarithmic growth phase were enzymatically dissociated with trypsin and subsequently reconstituted into a cell suspension. Then, 3 000 cells/well were seeded into 96 well plates. Following a 24-hour incubation period at 37 ℃, varying concentrations of DE-CDs were introduced into the respective wells, with DE-CDs-free samples serving as controls. At time points of 0, 24, and 48 hours, the plate was retrieved from the incubator, and 10 μL of CCK-8 solution was meticulously dispensed into each well. Following a 2 h incubation period with CCK-8, the absorbance at 450 nm was quantified utilizing a microplate reader.

### 1.6 Cell imaging

In order to assess the feasibility of Mn imaging within cellular contexts, both the human gastric cancer cell line MKN-45 and hepatic cell line LO2 were cultured and subsequently harvested. Subsequent to dual washes with PBS, the cells underwent fixation with 4% formaldehyde at room temperature for a duration of 10 min, succeeded by an additional two washes with PBS. Thereafter, the cells were subjected to staining through incubation with a mixture comprising $7.5\times10^{5}$ cells and 10 μL of freshly synthesized DE-CDs at 4 ℃ for a duration of 1 h. Upon completion of the incubation period, the resultant cells underwent triple rinsing with PBS to eradicate any unbound DE-CDs. Subsequently, the cells were resuspended in 20 μL of PBS and subjected to analysis utilizing confocal fluorescence microscopy (ZEISS Instruments, LSM 800).

## 2 Results and discussion

### 2.1 Design principle of $Mn^{2+}$-specific DE-CDs

To realize the detection of $Mn^{2+}$, a strategy was proposed for synthesizing DE-CDs and subsequently applied to investigate the cellular distribution of $Mn^{2+}$. As is well established, the selection of appropriate raw materials plays a crucial role in constructing $Mn^{2+}$-specific CDs endowed with distinctive dual-emission properties. Therefore, considering the way $Mn^{2+}$ binds to various proteins in living organisms, *L*-aspartic acid was first selected as the candidate for CDs synthesis since the surface structure strongly depends on the raw materials used. On the other

hand, directly synthesizing CDs with dual-emission properties can greatly simplify the process of constructing a fluorescence ratiometric sensor. Based on literature findings and our laboratory's prior experience, the incorporation of *p*-PD can substantially enhance the efficiency of synthesizing CDs with dual-emission properties (Bai et al., 2021). Simultaneously, employing *p*-PD as a raw material can effectively augment the nitrogen content of CDs, thereby significantly enhancing the binding affinity between carbon dots and $Mn^{2+}$, while also boosting the quantum yield of the synthesized CDs. Thus, *L*-aspartic acid and *p*-PD were chosen as raw materials for synthesizing Mn-specific DE-CDs.

## 2.2 Synthesis and characterization of DE-CDs

Based on the principle described above, the well-designed DE-CDs were synthesized through the simple hydrothermal method by mixing *L*-aspartic acid and *p*-PD together and heated at 200 ℃ for 12 h. After cooling to room temperature, the obtained DE-CDs were sequentially purified with filter paper and 0.22 μm membrane. To study the nature of the prepared CDs, morphologies and size were first characterized by transmission electron microscopy (TEM). As shown in Fig. 2a-c, synthesized DE-CDs are well dispersed in the solution and they exhibit quasi-spherical morphology with the particle size centered at 2.35 nm. The high-resolution TEM picture (Fig. 2b) reveals that the prepared DE-CDs contain a well-resolved lattice spacing of 0.21 nm which corresponds to the graphite-like structure. Besides, the crystallinity of DE-CDs was investigated by X-ray diffraction (XRD). As shown in Fig. 2d, a broad diffraction peak located around $2\theta = 22.4°$ was observed, demonstrating the (002) lattice spacing of a graphitic-like structure (Chen et al., 2023), which agrees well with the HR-TEM imaging.

Afterwards, the functional groups exposed on the surface of DE-CDs were characterized by the Fourier transform infrared (FT-IR) spectrum. As we can see from Fig. 2e, the broad and strong absorption at 3 135 $cm^{-1}$ is attributed to the stretching vibration of O—H and N—H; the absorption peak at 1 635 $cm^{-1}$ belongs to the bending vibration of N—H; the absorption at 1 580 and 824 $cm^{-1}$ indicates the presence of C═C, while the peak at 1370 $cm^{-1}$ belongs to the stretching vibration of C—N. These results indicate that the surface of synthesized DE-CDs contains multiple hydrophilic functional groups, including carboxyl, hydroxyl, and amino groups, significantly enhancing the water solubility of synthesized DE-CDs. In addition, X-ray photoelectron spectroscopy(XPS) was further used to study the surface composition and chemical state of the DE-CDs. Fig. 2f exhibits the full-scan XPS spectrum of the DE-CDs and the peaks at 285, 400 and 532 eV are consistent with C1s, N1s and O1s, indicating that as-synthesized DE-CDs are mainly composed of carbon, nitrogen and oxygen accounting for 72.62%, 15.45% and 11.93%, respectively (Lin et al., 2023). The high-resolution XPS spectra of each element are displayed in Fig. 2g-i. The high-resolution C1s spectrum (Fig. 2g) was deconvoluted into three peaks at 285, 286 and 288 eV, which contributed to the C═C, C—N, and C═O bond, respectively. Deconvolution of the high-resolution N1s spectrum yielded two peaks at 399 and 400 eV (Fig. 2h), corresponding to the pyridinic nitrogen (C—N) and amino nitrogen (N—H), respectively. The high-resolution O1s spectrum shows two peaks (Fig. 2i). One peak at 532 eV can be ascribed to C═O, while another peak at 533 eV is attributed to C—O. As expected, the XPS results were in agreement with the FTIR analysis.

Furthermore, the optical properties were systematically characterized. As shown in Fig. 3a, as-prepared DE-CDs show three UV-Vis absorption peaks at 240, 280 and 500 nm. The UV absorption peaks at 240 and 280 nm can be attributed to the $\pi$-$\pi$* or $n$-$\pi$* transition, respectively, while the broad peak at 500 nm may be related to the $n$-$\pi$* transition caused by the doping of heteroatoms (Yu et al., 2012). Because of this broad absorption peak at 500 nm, as-prepared DE-CDs appear to be orange (Fig. 3a insert). The fluorescence properties were further studied. Firstly, the synthesized DE-CDs were excited under different excitation wavelengths between 286−294 nm, and

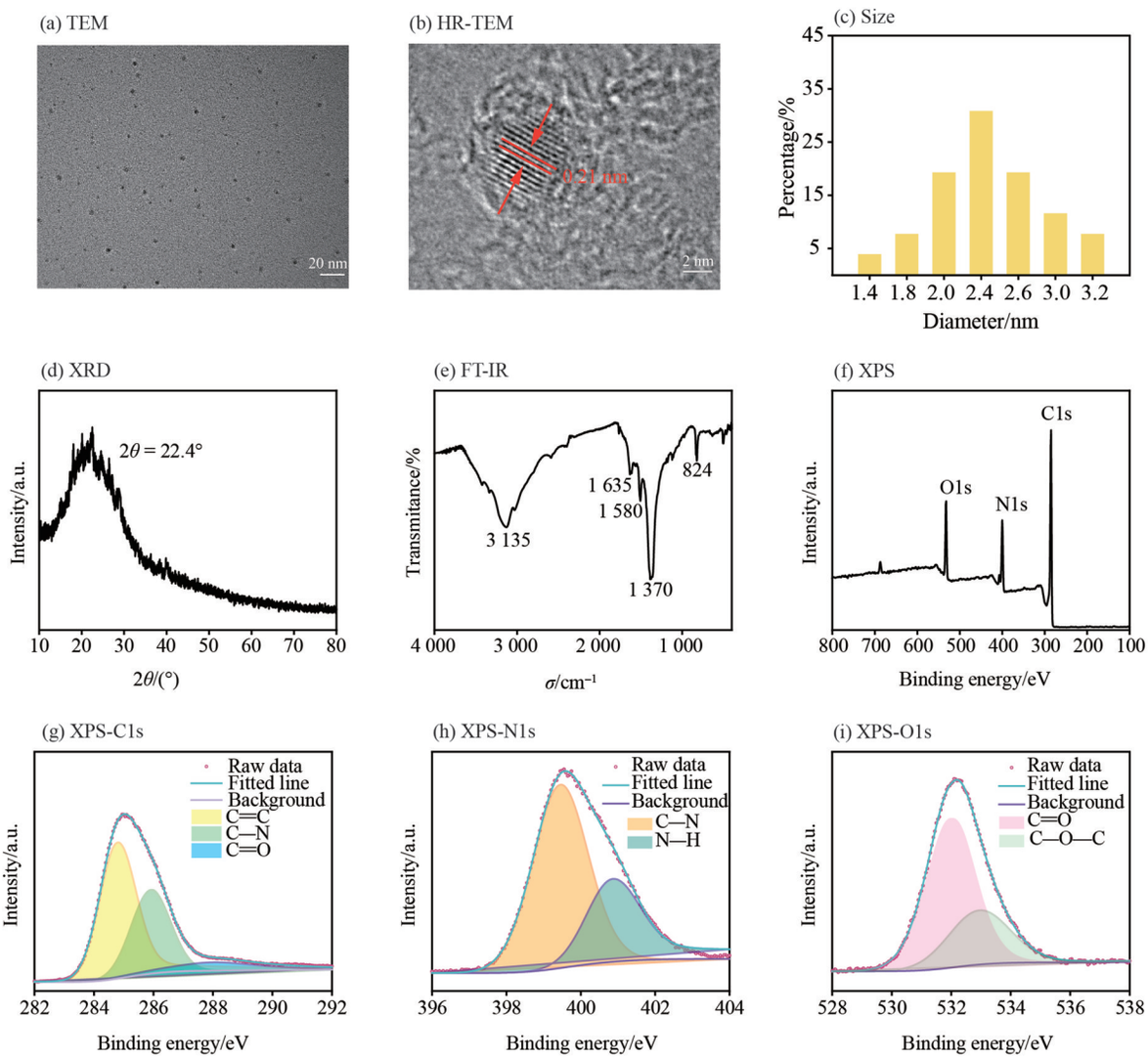


Fig. 2 Characterize the synthesized DE-CDs with different techniques

two well-resolved peaks centered at 350 and 610 nm were observed, indicating the synthesized CDs have excellent dual-emission properties since *p*-PD has been involved as raw materials (Fig. 3b). Interestingly, as the excitation wavelength increases, the fluorescence intensity at 350 nm basically remains unchanged, while the fluorescence intensity at 610 nm decreases. The position of the two peaks does not show any blue or red shift, demonstrating that the synthesized DE-CDs do not show wavelength dependence properties, which could be caused by the uniformly distributed particle size. Then, the excitation spectrum was scanned (Fig. 3c). Two excitation peaks at 235 and 290 nm were observed, exhibiting a mirror image with the emission spectrum, and the optimal excitation wavelength was set as $\lambda_{ex}$=290 nm for further use. Afterwards, the quantum yield was detected to be 4. 98% by using quinine sulfate as a reference (see Appendix table 1), and the lifetime of synthesized DE-CDs was detected to be 1. 85 ns (Fig. 3d). Based on these different characterizations stated above, the DE-CDs with excellent dual-emission properties were successfully synthesized, which could be further applied to construct a ratiometric sensor for the specific analytes.

## 2. 3 Constructing $Mn^{2+}$-specific ratiometric sensor

Based on the superior intrinsic dual-emission properties and abundant functional groups exposed on the surface of the synthesized DE-CDs, the feasibility of constructing the ratiometric sensor for $Mn^{2+}$ determination has been explored. Illustrated in Fig. 4a, the 3D fluorescence emission map of DE-CDs was

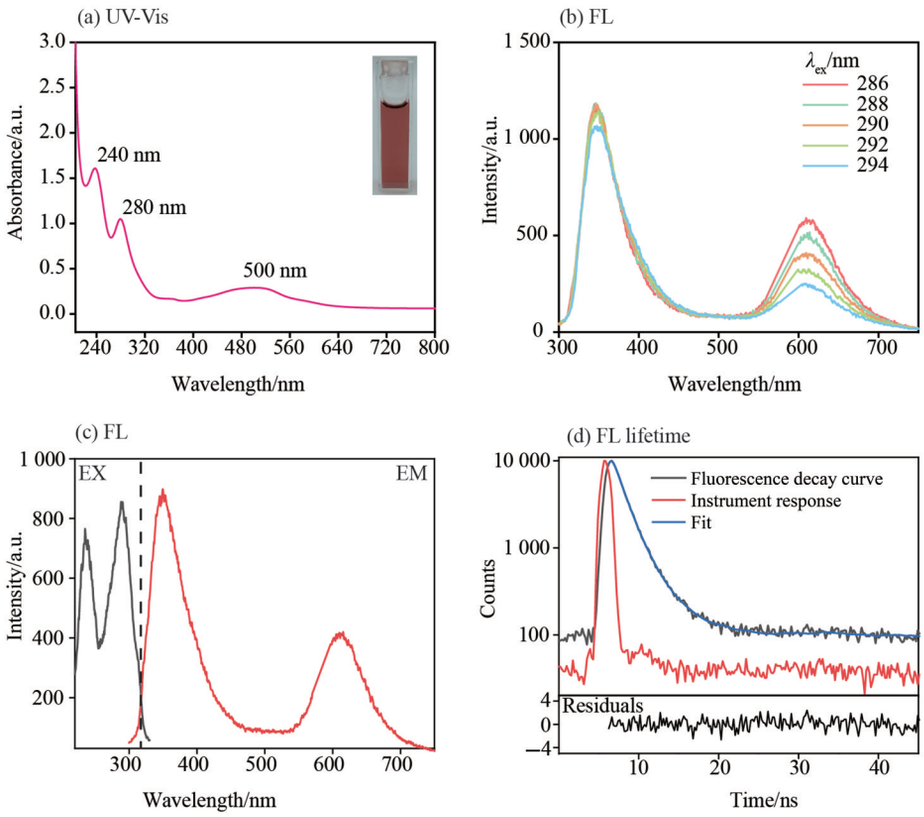


Fig. 3 Optical properties characterization of the synthesized DE-CDs

scanned, revealing two emission peaks at 350 and 610 nm, consistent with the emission spectrum. Upon the introduction of $Mn^{2+}$, the fluorescence intensity at 350 nm experienced a notable increase, while the signal at 610 nm remained stable. Thus, by employing the fluorescence signal at 350 nm as the responsive signal and the intensity at 610 nm as an internal reference, a ratiometric sensor for $Mn^{2+}$ detection can be established. The $F_{350}/F_{610}$ ratio exhibits a positive correlation with the concentration of $Mn^{2+}$ within a defined range, enabling the determination of $Mn^{2+}$ ions.

The potential sensing mechanism underlying the increase in fluorescence signal at 350 nm was further investigated. This phenomenon may be caused by the conjugation between $Mn^{2+}$ and the functional groups exposed on the surface of DE-CDs, thereby forming a structure with enhanced fluorescence efficiency. To verify this hypothesis, the UV-Vis absorption spectrum of the system was initially recorded both in the presence and absence of $Mn^{2+}$. As depicted in Fig. 4b, the UV absorption spectrum underwent significant changes upon the addition of $Mn^{2+}$. The absorption peak at 280 nm exhibited an increase, while the peak at 240 nm experienced a blue shift to 233 nm with enhanced absorption. This result suggested an increase in the $\pi$-$\pi$* or $n$-$\pi$* transition, which was responsible for the enhancement of the observed fluorescence signal at 350 nm (Mohagheghpour et al., 2022). Conversely, the broad absorption peak at 500 nm remains essentially unchanged after the addition of $Mn^{2+}$, possibly accounting for the stability of fluorescence intensity at 610 nm. Furthermore, the fluorescence lifetime was applied to investigate the possible mechanism. The fluorescence decay profile and its corresponding fitting parameters for the proposed system are illustrated in Appendix fig.1. The fluorescence lifetime of DE-CDs was determined to be 1.85 ns, markedly distinct from that of the system with $Mn^{2+}$ (1.91 ns), indicating that the interaction between DE-CDs and $Mn^{2+}$ may trigger the radiative recombination of excitations. Based on the aforementioned results, we infer that $Mn^{2+}$ may specifically conjugate with DE-CDs, thereby significantly altering the surface structure of DE-CDs and leading to fluorescence

enhancement at 350 nm.

As we know, the surface structure of DE-CDs is closely related to the selected precursor. The role of *p*-PD was examined by synthesizing control CDs, substituting *p*-PD with other commonly used raw materials. Firstly, control *o*CDs and *m*CDs were synthesized by substituting *p*-PD with its isomers, *o*-PD and *m*-PD, respectively. Apart from the altered precursors, all other synthesis conditions remained consistent with those of DE-CDs. As depicted in Appendix fig. 2a-b, only a single emission peak was observed, and the fluorescence intensity was quenched in the presence of $Mn^{2+}$. These results demonstrate that *o*CDs and *m*CDs could conjugate with $Mn^{2+}$ ions, however, paramagnetic $Mn^{2+}$ efficiently quenched the emission signals. Additionally, commonly employed raw materials such as ethylenediamine, glutathione, and formamide were employed as precursors to substitute *p*-PD. The results are shown in Appendix fig. 2c-e and none of these control CDs exhibit unique dual-emission properties, proofing the high importance of involving *p*-PD as the precursor in this system. More fascinatingly, these control CDs cannot even coordinate with $Mn^{2+}$ and generate coordination-induced enhancing/decreasing signals. Based on the aforementioned findings, it is proposed that $Mn^{2+}$ can efficiently conjugate with the binding scaffolds exposed on the surface of DE-CDs. The binding scaffolds are likely composed of carboxyl groups derived from *L*-aspartic acid and amino groups from *p*-PD, as the surface structure of DE-CDs is intrinsically linked to the chosen precursor. Upon $Mn^{2+}$ conjugation, a structure with enhanced $\pi$-$\pi^*$ and $n$-$\pi^*$ transitions emerged, thereby significantly increasing the UV-Vis absorption at 280 nm. Simultaneously, the fluorescence lifetime extended from 1.85 ns to 1.91 ns. In light of the presented findings, the hypothesized binding structure between $Mn^{2+}$ and the surface of DE-CDs is illustrated in Fig. 4c.

Since the analytical performance is closely related to the reaction condition between as-synthesized DE-CDs and $Mn^{2+}$, the influence of pH, buffer type/volume, and dosage of DE-CDs was investigated. Among these conditions, we first examined the influence of pH value, as it can directly affect the intrinsic fluorescence properties of DE-CDs through surface protonation and deprotonation processes. As the pH value decreased from 10.0 to 6.0, the fluorescence

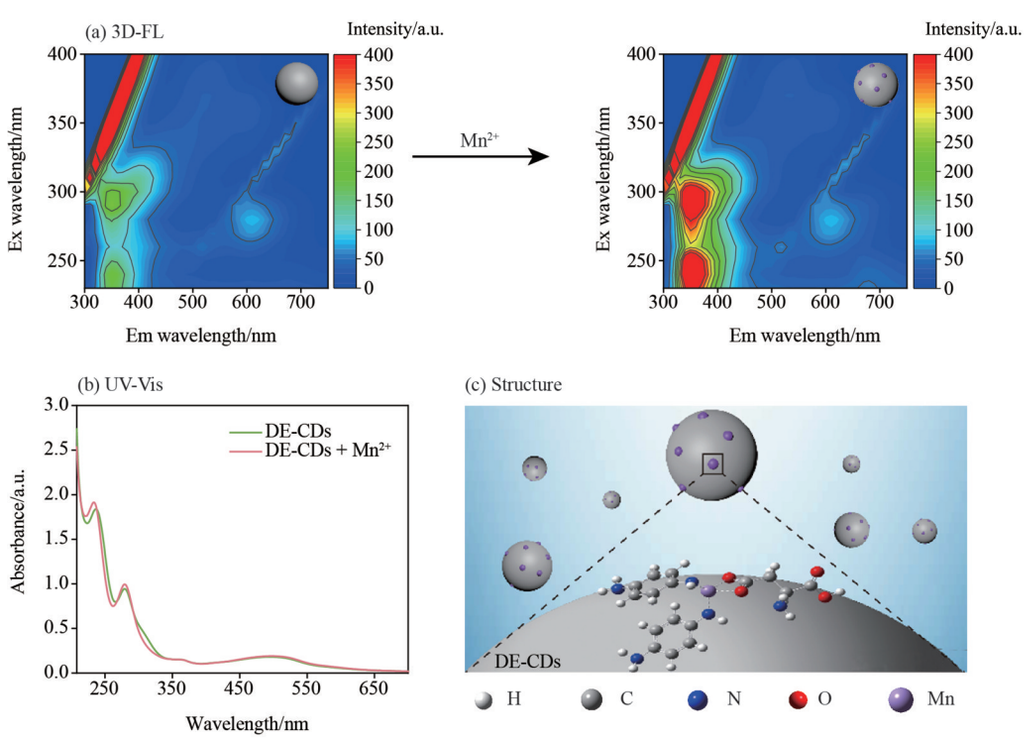


Fig. 4 The sensing mechanism of the proposed assay

signal at 350 nm increased; however, the excess $H^+$ in acidic conditions may also impede or compete with the $Mn^{2+}$ coordination process, thereby potentially affecting signal enhancement. As shown in Appendix fig. 3a-c, the highest $\Delta F_{350}/F_{610}$ value was achieved at pH 7. 0, thus, 30 μL Tris-HCl buffer (pH 7. 0) was utilized in the following assay to achieve better detection performance. Additionally, the fluorescence signal is closely linked to the concentration of the as-prepared DE-CDs, which was further optimized. As illustrated in Appendix fig. 3d, the $\Delta F_{350}/F_{610}$ value markedly increases as the volume increases from 100 to 200 μL; however, the $\Delta F_{350}/F_{610}$ value decreases upon further volume increase. The most significant difference of $\Delta F_{350}/F_{610}$ value is observed at 200 μL, thus 200 μL is selected in the following experiments. Based on the aforementioned results, the $Mn^{2+}$ determination process was performed in a system containing 200 μL of as-prepared DE-CDs and 30 μL of Tris-HCl buffer (pH 7. 0).

The analytical performance of this ratiometric assay was then investigated under optimal conditions. The fluorescence emission spectra of DE-CDs were recorded in the presence of different concentrations of $Mn^{2+}$. As shown in Fig. 5a, the fluorescence intensity at 350 nm is gradually raised with the increased concentration of $Mn^{2+}$, while the signal at 610 nm remains stable. Thus, by employing the fluorescence intensity at 350 nm as the responsive signal and 610 nm as the internal reference, a ratiometric sensor for $Mn^{2+}$ analysis was established. Fig. 5b illustrates that the $F_{350}/F_{610}$ value exhibits a strong linear relationship with $Mn^{2+}$ concentrations ranging from 0. 9 to 15 μmol/L, with the linear equation determined as $y$=0. 344 62$x$+2. 4 ($R^2$=0. 992). In this linear equation, $x$ and $y$ represent the concentration of $Mn^{2+}$ and the signal ratio of DE-CQDs at 350 nm and 610 nm, respectively. Under the optimal conditions, the limit of detection (LOD) is calculated to be 61 nmol/L based on the $3\sigma/k$ theory, which is comparable to other work (see Appendix table 2) and lower than the $Mn^{2+}$ content in whole blood and cellular organelles. These findings demonstrate that the proposed assay exhibits exceptional sensitivity, making it suitable for applications in biological systems and cellular imaging.

Subsequently, the stability of the proposed ratiometric assay was further explored. To test the stability of the proposed assay, the constructed system was challenged with different concentrations of NaCl or KCl. As shown in Appendix fig. 4, the $\Delta F_{350}/F_{610}$ value remained stable even when 30 mmol/L NaCl or KCl was added into the system, exhibiting a strong resistance to salt interference. Additionally, the system's stability was assessed by subjecting it to varying incubation times. The results are depicted in Fig. 5c, indicating a stable $\Delta F_{350}/F_{610}$ value even as the incubation time extends from 10 mins to 480 mins (8 h). This result also demonstrates that the reaction between $Mn^{2+}$ and DE-CDs is fast and can be finished within 10 mins, which provides powerful evidence to construct a rapid analysis method for $Mn^{2+}$.

In addition to sensitivity and stability, specificity stands as another critical property inherent in analytical methodologies. In order to assess its specificity, the proposed assay underwent initial testing with various metal cations and anions, including $Ca^{2+}$, $Mg^{2+}$, $Na^+$, $K^+$, $Zn^{2+}$, $Ba^{2+}$, $Pb^{2+}$, $Co^{2+}$, $Cd^{2+}$, $F^-$, $Br^-$, $I^-$ and $ClO^-$. As depicted in Fig. 5d, solely $Mn^{2+}$ elicited a fluorescence signal enhancement at 350 nm, whereas all other specimens manifested a signal akin to that of the blank sample. These results demonstrate that the proposed ratiometric assay is highly specific towards $Mn^{2+}$ over other interferents, showing great potential for analysis in real samples.

To further validate the anti-interference capability of the proposed system in intricate biological settings, we examined the signal response of the system through the mixing of $Mn^{2+}$ with various metal ions and biomolecules, including $Ca^{2+}$, $Mg^{2+}$, $Zn^{2+}$, $Ba^{2+}$, $Na^+$, $K^+$, $Ag^+$, glycine, serine, leucine, threonine, methionine, valine and glucose. The concentration of these interferents is fixed at 700 μmol/L, which is 100 times higher than $Mn^{2+}$. As illustrated in Table 1, the observed relative error falls within the range of ±5. 0%, unequivocally indicating that the presence of

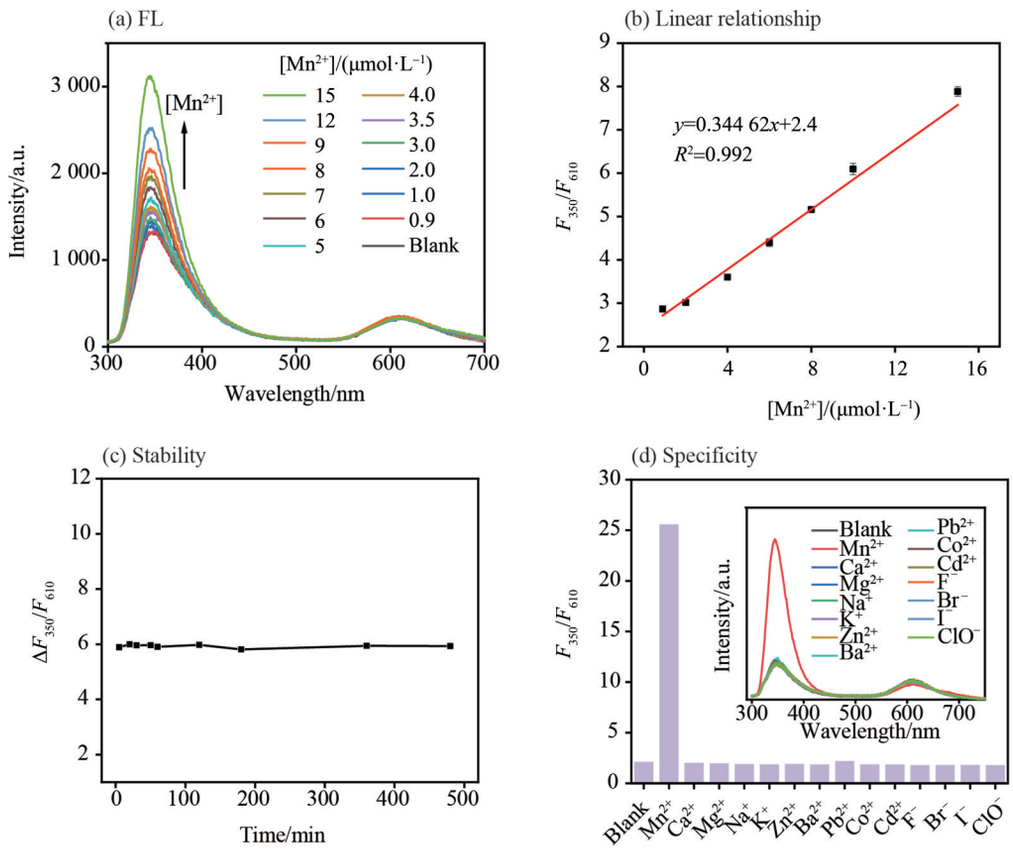


Fig. 5 Analytical performance of the proposed ratiometric assay

Table 1 Effect of interfering ions and biomolecules on the proposed system

| Interferent | Interference folds | Err. /% | Interferent | Interference folds | Err. /% |
|---|---|---|---|---|---|
| $Ca^{2+}$ | 100 | −1. 4 | Glycine | 100 | 0. 63 |
| $Mg^{2+}$ | 100 | −0. 96 | Serine | 100 | −0. 32 |
| $Na^{+}$ | 100 | −0. 24 | Leucine | 100 | 4. 30 |
| $K^{+}$ | 100 | −2. 2 | Threonine | 100 | −0. 84 |
| $Zn^{2+}$ | 100 | 3. 6 | Methionine | 100 | 4. 20 |
| $Ba^{2+}$ | 100 | 2. 7 | Valine | 100 | −3. 30 |
| $Ag^{+}$ | 100 | 0. 74 | Glucose | 100 | 3. 20 |

these interfering substances does not impede the determination of $Mn^{2+}$, despite their concentration being 100 times that of $Mn^{2+}$. Based on these analytical performance evaluations tested above, this proposed ratiometric assay exhibits high sensitivity, strong stability, and excellent specificity towards $Mn^{2+}$, rendering it suitable for $Mn^{2+}$ analysis in biological specimens.

## 2. 4 Real sample application and cell imaging

A practical assay should be applicable for target analysis in complex environments. In this section, the $Mn^{2+}$ content in river sample were initially evaluated using the proposed assay, followed by a comparative analysis with the results derived from the national standard method, formaldehyde oxime spectrophotometry (HJ/T344−2007). The river samples were collected from the Yan River, a significant fluvial system in the region. Large particulate impurities in the river sample were initially removed using a double layer of filter paper. Subsequently, a 0. 22 μm filter was employed to eliminate finer particulate impurities, thereby ensuring the samples' purity.

Probably due to the exceedingly low concentration, both methods failed to detect $Mn^{2+}$ in the river sample. To further evaluate the accuracy of the proposed assay, 1. 60, 2. 00 and 3. 00 μmol/L of standard $Mn^{2+}$ was added into the real sample and the additional concentrations were tested to be 1. 57, 2. 07 and 2. 96 μmol/L, respectively, with a good recovery ranging from 98. 12% to 103. 50%, which indicate the high accuracy and reliability of the proposed assay (Table 2). Subsequently, the DMEM cell culture medium, containing a high concentration of amino acids, salt, and various biomolecules, was used as the model to mimic the complex biological fluid. The analytical performance of the constructed assay was evaluated in this mimic biological fluid by adding diluted DMEM into the detection system containing various concentrations of $Mn^{2+}$. The results shown in Table 2 suggest that the proposed assay works well in this complex DMEM matrix. Based on the calibration curve constructed at the same time, the content of spiked $Mn^{2+}$ was tested to be 1. 61, 2. 01 and 3. 08 μ mol/L, respectively, with the calculated recovery ranging from 100. 50% to 102. 70%. More fascinatingly, even if complete cell culture (DMEM + 10% FBS) was used as the mimicked biological fluid, the analytical performance was not affected. These results demonstrate that the proposed ratiometric assay shows high reliability and accuracy which could be successfully applied for $Mn^{2+}$ analysis in complex biological samples.

Table 2 Recovery results of the determination of $Mn^{2+}$ in real sample（$n$ = 5）

| Sample | Spectrophotometry/（μmol·L$^{-1}$） | This method | | | | |
|---|---|---|---|---|---|---|
| | | Content/（μmol·L$^{-1}$） | Added/（μmol·L$^{-1}$） | Found/（μmol·L$^{-1}$） | Recovery/% | RSD/% |
| River sample | ND | ND | 1. 60 | 1. 57 | 98. 12 | 3. 1 |
| | | | 2. 00 | 2. 07 | 103. 50 | 1. 5 |
| | | | 3. 00 | 2. 96 | 98. 67 | 2. 9 |
| DMEM | ND | ND | 1. 60 | 1. 61 | 100. 60 | 1. 8 |
| | | | 2. 00 | 2. 01 | 100. 50 | 1. 5 |
| | | | 3. 00 | 3. 08 | 102. 70 | 1. 0 |
| DMEM +10% FBS | ND | ND | 1. 60 | 1. 60 | 100. 00 | 1. 2 |
| | | | 2. 00 | 2. 04 | 102. 00 | 1. 0 |
| | | | 3. 00 | 2. 98 | 99. 33 | 1. 5 |

Note：“ND” represent “Not Detected”.

Moreover, the feasibility of applying synthesized DE-CDs as an effective probe for $Mn^{2+}$ imaging in cells was investigated. Before the cell imaging, CCK8 assays were performed to estimate the cytotoxicity of the prepared DE-CDs. As shown in Appendix fig. 5, the survival rate of the MKN-45 cells is over 90%, which indicates low toxicity and excellent biocompatibility of the synthesized particles. Afterwards, MKN-45 and LO2 cells were treated with DE-CDs followed by confocal microscope imaging (Fig. 6). It is obvious that blue fluorescence could be observed, demonstrating the as-prepared DE-CDs could be applied for cell imaging. When 5 μmol/L $Mn^{2+}$ was introduced and incubated with the above-stated imaging system, $Mn^{2+}$ could efficiently conjugate to the surface of DE-CDs, thereby modifying their surface structure and markedly enhancing their fluorescence emission. Fig. 6 clearly demonstrates that the blue fluorescence emission from MKN-45 and LO2 cells is significantly enhanced upon the addition of DE-CDs and $Mn^{2+}$ to the system, likely due to the conjugation of $Mn^{2+}$ with DE-CDs. It should be noted that the prepared DE-CDs can be excited across a quite broad wavelength range (Fig. 4a), consequently, in cases where some biomolecules including tryptophan, and tyrosine cause interference in the determination, an

alternative excitation wavelength can be selected. In addition, the quantification process was performed according to the fluorescence enhancement caused by the coordination between DE-CDs and $Mn^{2+}$ cation, therefore, the autofluorescence signal from cells can be regarded as background signals and adjusted through the blank sample. Based on the results presented and discussed above, the prepared DE-CDs could be successfully applied for $Mn^{2+}$ imaging and quantification in cells.

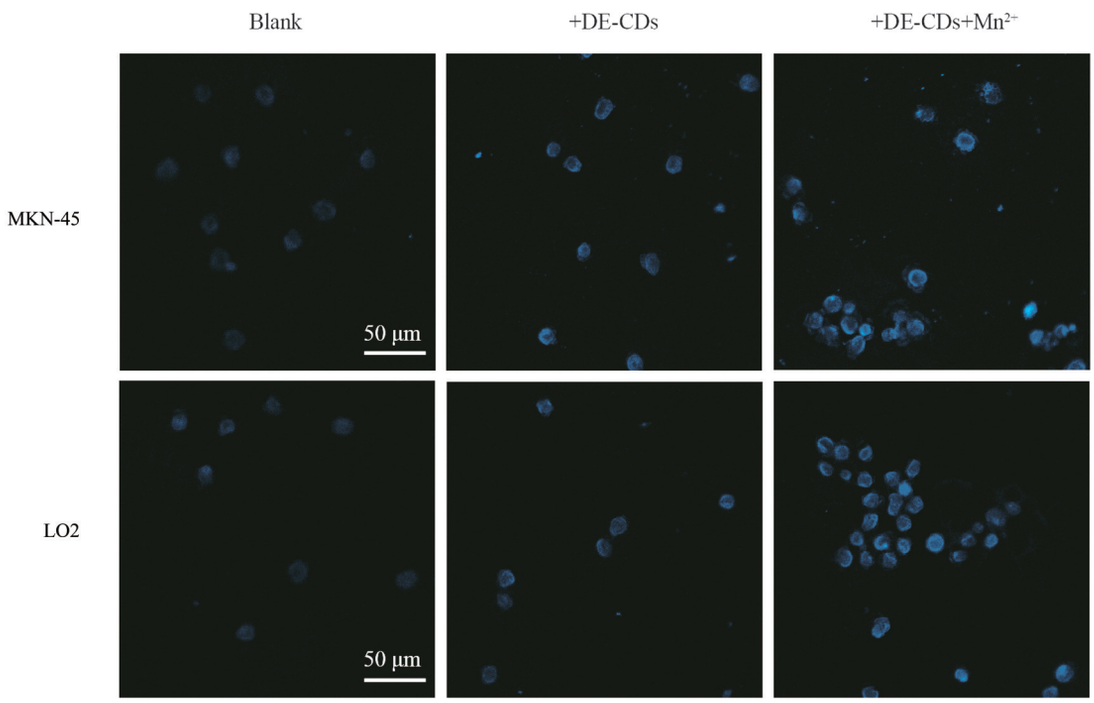


Fig. 6 Cellular imaging of MKN-45 and LO2 cells by confocal laser scanning microscope

## 3 Conclusions

In summary, we successfully synthesized the DE-CDs and constructed a simple, rapid, and practical ratiometric approach to selectively detect $Mn^{2+}$. The DE-CDs with unique dual-emission properties were first synthesized through the simple hydrothermal method by using *L*-aspartic acid and *p*-PD as raw materials. In the presence of $Mn^{2+}$, the fluorescence intensity of the DE-CDs at 350 nm was significantly enhanced while the signal at 610 nm remained stable. Therefore, a ratiometric sensor for $Mn^{2+}$ determination was constructed and the sensing mechanism was further investigated. Based on this special $Mn^{2+}$-induced ratiometric sensing approach, this sensor achieved excellent linear relationship and outstanding sensitivity, selectivity, and stability, which could be further applied in complex biological samples and cellular imaging. We believe that the present data and method considerably extend the current knowledge and provide us with a novel route in establishing the DE-CDs-based ratiometric sensor for $Mn^{2+}$ analysis.

## 参考文献:

BAI J, YUAN G, ZHU Y, et al, 2021. Study on the origin of fluorescence by using dual-emission carbon dots[J]. J Phys Chem C, 125(33): 18543-18551.

CAI L X, WANG Y, CHEN Y Y, et al, 2023. Manganese(II) complexes stimulate antitumor immunity via aggravating DNA damage and activating the cGAS-STING pathway[J]. Chem Sci, 14(16): 4375-4389.

CHAUDHARI K G, PATIL P O, NANGARE S N, et al, 2024. Exploring the significance of carbon quantum dots and graphene quantum dots in sarcosine sensing: A key

biomarker for prognosticating prostate cancer[J]. Chem Select, 9(29): e202401643.

CHEN J, XIA X, LI P, et al, 2023. A facile "off-on" fluorescence sensor for pentachlorophenol detection based on natural N and S co-doped carbon dots from crawfish shells[J]. Food Chem, 405(30): 134802.

CHEN Y J, SUN J, LUO M P, et al, 2024. Quantifying the viability of lactic acid bacteria using ratiometric fluorescence assays[J]. Microchem J, 206: 111485.

DAS S, KHATUA K, RAKSHIT A, et al, 2019. Emerging chemical tools and techniques for tracking biological manganese[J]. Dalton Trans, 48(21): 7047-7061.

FAN H H, MCGHEE C E, LAKE R J, et al, 2023. A highly selective Mn(II)-specific DNAzyme and its application in intracellular sensing[J]. JACS Au, 3(6): 1615-1622.

GOSHISHT M K, TRIPATHI N, PATRA G K, et al, 2023. Organelle-targeting ratiometric fluorescent probes: Design principles, detection mechanisms, bio-applications, and challenges[J]. Chem Sci, 14(22): 5842-5871.

HORNING K J, CAITO S W, TIPPS K G, et al, 2015. Manganese is essential for neuronal health[J]. Annu Rev Nutr, 35(1): 71-108.

KWAKYE G, PAOLIELLO M, MUKHOPADHYAY S, et al, 2015. Manganese-induced parkinsonism and parkinson's disease: shared and distinguishable features[J]. Int J Environ Res Public Health, 12(7): 7519-7540.

LI J, CEN Y, LI Y, 2018. The research advances in the mechanism of manganese-induced neurotoxicity[J]. Toxin Rev, 38(1): 54-60.

LIN S Q, JIA B Z, LUO W, et al, 2023. Controllable formation of polydopamine on carbon dots for ultrasensitive detection of alkaline phosphatase and ratiometric fluorescence immunoassay of benzocaine[J]. Food Chem, 426(15): 136582.

LV M, CHEN M, ZHANG R, et al, 2020. Manganese is critical for antitumor immune responses via cGAS-STING and improves the efficacy of clinical immunotherapy[J]. Cell Res, 30(11): 966-979.

MIZUNUMA M, SUZUKI M, KOBAYASHI T, et al, 2023. Development of $Mn^{2+}$-specific biosensor using G-quadruplex-based DNA[J]. Int J Mol Sci, 24(14): 11556.

MOHAGHEGHPOUR E, FARZIN L, GHOORCHIAN A, et al, 2022. Selective detection of manganese (II) ions based on the fluorescence turn-on response via histidine functionalized carbon quantum dots[J]. Spectrochimi Acta A, 279(15): 121409.

NGEONTAE W, CHAIENDOO K, NGAMDEE K., et al, 2022. A highly selective fluorescent sensor for manganese (II) ion detection based on N, S-doped carbon dots triggered by manganese oxide[J]. Dyes Pigm, 203: 110325.

POURJAVID M R, ARABIEH M, YOUSEFI S R, et al, 2016. Interference free and fast determination of manganese(II), iron(III) and copper(II) ions in different real samples by flame atomic absorption spectroscopy after column graphene oxide-based solid phase extraction[J]. Microchem J, 129: 259-267.

SHI Y H, SHI Y, WANG Z Y, et al, 2023. Glucose-responsive mesoporous prussian blue nanoprobes coated with ultrasmall gold and manganese dioxide for magnetic resonance imaging and enhanced antitumor therapy[J]. Chen Eng J, 453: 139885.

TUERHONG M, YANG X, XUE B Y, 2017. Review on carbon dots and their applications[J]. Chinese J Anal Chem, 45(1): 139-150.

WANG F H, DONG X Z, ZUO Y J, et al, 2024. Effectively enhancing red fluorescence strategy and bioimaging applications of carbon dots[J]. Mater Today Phys, 41: 101332.

WANG Y, ZHANG C, CHEN X, et al, 2016. Ratiometric fluorescent paper sensor utilizing hybrid carbon dots-quantum dots for the visual determination of copper ions[J]. Nanoscale, 8(11): 5977-5984.

YU P, WEN X, TOH Y R, et al, 2012. Temperature-dependent fluorescence in carbon dots[J]. J Phys Chem C, 116(48): 25552-25557.

ZHANG J, CHEN Y, QI J, et al, 2024. A paper-based ratiometric fluorescence sensor based on carbon dots modified with $Eu^{3+}$ for the selective detection of tetracycline in seafood aquaculture water[J]. Analyst, 149(5): 1571-1578.

ZHANG Y C, LI C J, SUN L B, et al, 2021. Defects coordination triggers red-shifted photoluminescence in carbon dots and their application in ratiometric Cr(VI) sensing[J]. Microchem J, 169: 106552.

ZHANG Z, SHANG C, ZHAO W, et al, 2022. 3,3′,5,5′-Tetramethylbenzidine and polyetherimide decorated silver nanoparticles for colorimetric $Mn^{2+}$ ions detection in aqueous solution[J]. Chem Pap, 76(11): 7253-7260.

# 基于双发射碳量子点的比率型荧光探针在 $Mn^{2+}$传感与细胞成像中的应用

张越诚[1]，马静[1]，孙凌波[2]，陈飞[3]，张诗雨[1]，张雨晗[2]，李淼[1]，张雅蓉[1]，马红燕[1]

1. 延安大学化学与化工学院，陕西 延安 716000
2. 延安大学延安医学院，陕西 延安 716000
3. 新正检验检测有限公司，新疆 乌鲁木齐 830000

**摘要：** Mn作为一种人体必需的微量元素，在众多生命过程中都发挥着重要作用。近期研究发现，$Mn^{2+}$可独立激活cGAS-STING通路，显著提高免疫治疗效果。但由于$Mn^{2+}$特异性分子探针的缺失，导致$Mn^{2+}$介导cGAS-STING通路免疫调控分子机制的相关研究滞后。因此，急需构建活细胞内$Mn^{2+}$的检测与成像方法。本文使用天冬氨酸与对苯二胺为原材料，通过一步水热法合成了具有双发射特性的碳量子点。当$Mn^{2+}$加入碳量子点溶液时，碳量子点在350 nm处的荧光发射峰显著增强，而其在610 nm处的发射强度基本保持不变。因此，使用350、610 nm处的信号值分别作为响应信号与参比信号，便可构建特异性识别$Mn^{2+}$的比率型荧光探针。在最优的条件下，该探针在0.9~15 μmol/L之间具有良好的线性范围，检出限为61 nmol/L。该探针得益于$Mn^{2+}$介导的比率型荧光信号响应，使其具有出色的灵敏度、特异性以及稳定性，能进一步应用复杂生物样品中$Mn^{2+}$的分析检测与细胞成像，对$Mn^{2+}$介导cGAS-STING通路免疫调控分子机制的研究具有潜在的应用价值。

**关键词：** $Mn^{2+}$；碳量子点；比率型；细胞成像；荧光

（责任编辑　张　冰）

·喜　讯·

# 本刊主编胡建勋教授荣获“广东省劳动模范”称号

4月29日上午，2025年广东省庆祝“五一”国际劳动节暨劳动模范、先进工作者和先进集体表彰大会在广州举行。354位广东省劳动模范、40位广东省先进工作者和97个广东省先进集体受到表彰。《中山大学学报（自然科学版中英文）》主编胡建勋教授荣获“广东省劳动模范”称号。胡建勋教授，博士生导师，享受国务院政府特殊津贴。致力于辛拓扑与数学物理的前沿研究并取得丰硕成果，合作建立了辛流形的双有理等价二分法（单直纹或非单直纹）的分类，催生双有理辛几何成为研究新方向，被国际同行誉为“奠基性工作”。获2023年度国家自然科学奖二等奖（第一完成人），2020年教育部高等学校科学研究优秀成果奖自然科学奖一等奖（第一完成人），曾主持国家杰出青年科学基金项目、国家自然科学基金重点项目和国家重点研发计划项目等，先后入选教育部“新世纪优秀人才支持计划”、人社部“新世纪百千万人才工程”国家级人选、广东省特支计划百千万工程领军人才。


1995年9月任教至今，始终坚守在教育教学一线，扎根讲台30载，以言传身教培养了一批又一批的数学学子。曾获广东省教学成果奖二等奖、广东省“南粤优秀教师（教坛新秀）”，任教的本科基础课程《数学分析》获评为国家精品课程；作为基础数学教师团队核心成员2023年入选第三批“全国高校黄大年式教师团队”；作为国家级平台粤港澳应用数学中心主要成员，聚焦制约行业发展的“卡脖子”数学问题，推动科研成果转化，为服务国家战略和区域经济发展、粤港澳大湾区建设提供了智力支持。

2019年担任《中山大学学报（自然科学版中英文）》主编以来，胡建勋教授带领编辑团队深入科研第一线，积极进行组稿约稿，提升学术质量；增设“特约综述（论文）”“学术前沿”“名家风范”栏目，聚焦学术热点，增强学术引导力；全面推行排版定稿网络优先发表，缩短学术成果发表周期；变更期刊文种为中英文，提升期刊的国际影响力；构建了论文投审稿、编辑加工、出版传播全流程数字化的云出版服务平台，使期刊的影响力持续攀升，2022年获首届广东出版政府奖期刊奖。

《中山大学学报（自然科学版中英文）》编辑部